Intelligence & Control
https://www.sciltp.com/journals/ic

Article

Predictive Fault-Tolerant Control of an Aero-Engine Actuator Based on an N-Step Extended State Observer

Yang Liu [1], Shuoshuo Liu [1], Ning Xu [2,*] and Xudong Zhao [1]

[1] Key Laboratory of Intelligent Control and Optimization for Industrial Equipment of Minstry of Education, Dalian University of Technology, Dalian 116081, China
[2] College of Information Science and Technology, Bohai University, Tianjin 121013, China
* Correspondence: hpxuning@163.com

How To Cite: Liu, Y.; Liu, S.; Xu, N.; et al. Predictive Fault-Tolerant Control of an Aero-Engine Actuator Based on an N-Step Extended State Observer. *Intelligence & Control* **2025**, *1*(1), 1.

Received: 8 March 2025
Revised: 1 April 2025
Accepted: 17 April 2025
Published: 20 May 2025

Abstract: This paper addresses the composite control problem of aero-engine systems under actuator faults and input saturation constraints. A novel n-step extended state observer (ESO) is proposed to precisely estimate actuator fault signals. Based on this estimation, a model predictive control (MPC) framework is developed to optimize system performance while explicitly addressing input saturation. Unlike conventional observer-based MPC strategies that depend on feedback compensation, the proposed approach directly integrates the estimated fault signal into the predictive model, enabling simultaneous fault estimation and compensation. This integration significantly enhances fault tolerance and control accuracy. Simulation results demonstrate that the proposed method effectively estimates actuator faults and ensures safe, reliable, and efficient aero-engine operation within predefined safety constraints. The approach is shown to be robust and capable of maintaining system stability under adverse conditions.

Keywords: aero-engine; actuator fault; n-step extended state observer; model predictive control

1. Introduction

Aviation safety is of critical importance in the aerospace industry, particularly in the design and control of aero-engine systems. Actuators are essential for regulating key operational parameters, such as fuel supply and rotor speed, to ensure stable and efficient engine performance. However, harsh operating conditions and prolonged component aging can result in actuator faults, which may degrade control accuracy and, in severe cases, lead to system failures. As a result, fault-tolerant control (FTC) for actuator faults in aero-engine systems has emerged as a significant area of research [1–3]. Despite significant advancements, the development of effective fault-tolerant control (FTC) strategies for aero-engines remains challenging due to the inherent complexity of engine dynamics, stringent safety requirements, and the persistent demand for optimal performance. These challenges underscore the need for innovative approaches that can simultaneously enhance system reliability and robustness under various fault conditions while maintaining operational efficiency.

Fault detection and estimation through observer-based adaptive methods with feedback compensation is extensively utilized in modern control systems [4, 5]. Among the most widely adopted observers for fault estimation are the H_∞ observer [6–8], Luenberger observer [9, 10], adaptive observer [11, 12], and extended state observer (ESO) [13, 14]. Notably, ESO-based approaches model actuator faults as additional state variables, facilitating the development of fault-tolerant control strategies that ensure closed-loop system stability. Stability analysis is generally performed using Lyapunov theory to validate the feasibility of both fault reconstruction and fault-tolerant control. This theoretical framework provides a robust foundation for ensuring system reliability and performance under fault conditions. While observer-based methods are effective in predicting faults, detecting fault signals, and mitigating external disturbances, the accuracy of fault estimation plays a critical role in determining overall control performance. To enhance estimation accuracy, Wang [15] proposed a finite-time extended state observer for estimating the lumped disturbance caused by actuator faults in spacecraft systems. A novel bounded barrier Lyapunov function (BLF) was introduced to address singularities and excessive control efforts associated with traditional BLF methods and homeomorphic mapping techniques in the presence of actuator faults. Furthermore, Huang [16] developed a k-step fault estimation observer that utilizes historical fault information over k steps to more precisely characterize fault dynamics in terms of both magnitude and shape. Qi [17] proposed an advanced fault estimation methodology, introducing an integral compensation function observer to estimate disturbances in uncertain systems, this approach effectively addresses the limitations associated with conventional linear extended state observers, and a significant improvement in estimation accuracy is achieved. These advancements collectively contribute to the development of more robust and reliable fault-tolerant control strategies.

The design of fault-tolerant controllers is critical for enhancing actuator fault resilience in aero-engine control systems. Based on fault estimation, Li [18] proposed an output feedback-based fault-tolerant control (FTC) strategy, where sufficient conditions for both the observer and controller are formulated using linear matrix inequalities (LMIs) to ensure closed-loop system stability. However, the effectiveness of feedback-based FTC strategies is heavily reliant on model accuracy, and their performance can degrade significantly under parameter variations and external disturbances. To address these limitations, sliding mode control (SMC) has been widely adopted due to its robustness against model uncertainties and external perturbations. Through the appropriate design of the sliding mode surface, SMC enables rapid control adaptation and ensures system stability under varying dynamic conditions [19, 20]. Nevertheless, SMC lacks predictive capabilities, which restricts its effectiveness in handling input constraints and optimizing overall control performance. To overcome this drawback, model predictive fault-tolerant control (MPFTC) integrates model predictive control (MPC) with fault-tolerant mechanisms, explicitly accounting for system constraints while compensating for actuator faults. Zhang [21] proposed an MPC framework based on Quantum-behaved Particle Swarm Optimization (QPSO) with speed-constrained optimization for the Human Occupied Vehicle (HOV) system, effectively mitigating speed jumps caused by thruster faults and achieving smooth dynamic tracking. Similarly, Shi [22] addressed actuator random failures in discrete-time linear systems by constructing a transition probability matrix to model state evolution.A robust predictive fault-tolerant switching control strategy is developed to ensure system stability by leveraging historical data and system dynamics for fault prediction. The proposed predictive capabilities significantly enhance system resilience, improve fault-tolerant performance, and contribute to the safe and efficient operation of aero-engine control systems [23, 24].

As the core of modern aircraft propulsion systems, twin-spool turbofan engines' control system reliability directly impacts flight safety and operational economics. With continuously increasing performance demands, critical actuators such as low-Pressure Compressor Variable Stator Vanes (VSV) and Fuel Metering Units (FMU) are facing increasingly severe operating conditions. According to statistics from the International Aviation Safety Database , 43% of engine in-flight shutdown incidents caused by actuator faults over the past five years originated from actuator jamming or position feedback anomalies, with VSV system failures accounting for as much as 28%.

Motivated by the aforementioned challenges and advancements, this paper proposes a model MPFTC strategy based on an n-step ESO to address actuator faults in aero-engine control systems. The key contributions of this work are summarized as follows:

(1) Building upon conventional ESO methodologies, the proposed n-step ESO significantly enhances the accuracy of fault signal estimation through multi-step estimation . Additionally, the parameter n can be customized to align with the specific dynamics of the system, thereby improving the observer's adaptability and practical applicability.

(2) Unlike traditional observer-based fault-tolerant control strategies that depend exclusively on feedback compensation, the proposed approach directly incorporates the estimated fault signal into the predictive model. This integration enables simultaneous fault estimation and prediction, thereby enhancing the controller's responsiveness and improving the fault tolerance of the aero-engine system.

(3) The proposed fault-tolerant control scheme explicitly addresses actuator saturation constraints, ensuring safe and reliable engine operation while maintaining optimal performance under faulty conditions.

2. Main Result

2.1. Linear Modeling of an Aero-Engine

In this study, a two-shaft engine is modeled, with the engine rotor being the only energy storage component considered. Since the thermal inertia of the component is substantially smaller than that of the rotor, non-stationary heat transfer between the hot component, the rotor, and the surrounding medium is neglected. Under these assumptions, the dynamic behavior of the engine is governed by the equilibrium equations of the two rotors, expressed as:

$$\begin{cases} \frac{\pi}{30} J_H \frac{dn_H}{d_t} = \triangle M_H \\ \frac{\pi}{30} J_L \frac{dn_L}{d_t} = \triangle M_L \end{cases}, \tag{1}$$

where J_H and J_L denote the moments of inertia of the engine's low-pressure and low-pressure rotors, respectively, and ΔM_H and ΔM_L represent the residual moments of the low-pressure and low-pressure rotors, respectively. Based on the engine operating principles, the residual moments of the low-pressure and low-pressure rotors are defined as:

$$\begin{cases} \triangle M_H = \triangle M_H(n_H, n_L, q_{m,f}, A_8, p_2, T_2) \\ \triangle M_L = \triangle M_L(n_H, n_L, q_{m,f}, A_8, p_2, T_2) \end{cases}. \tag{2}$$

For simplicity in analysis, it is assumed that the flight conditions remain constant. Equation (2) is linearized, and the linear state-space equations of the engine are derived by extracting power from the low-pressure and low-pressure rotors. The engine input is sequentially varied within small ranges around the steady-state operating point, and the variations in the rotational speeds of the low- and low-pressure rotors, along with other parameters, are calculated through a balancing process as follows:

$$\begin{cases} \dot{x}(t) = Ax(t) + Bu(t) + Cf_a(t) \\ y(t) = C_m x(t) \end{cases}, \tag{3}$$

where $x = \begin{bmatrix} \Delta n_H & \Delta n_L \end{bmatrix}^T$, with Δn_H and Δn_L representing the variations in the low-pressure and low-pressure rotor speeds, respectively. Here, $u(t)$ denotes the change in fuel quantity, and $f_a(t)$ represents the actuator fault signal.

Discretizing the system (2) with respect to the sampling period T results in the following discrete system model:

$$\begin{cases} x(k+1) = \Phi x(k) + \Gamma u(k) + \Gamma_a f_a(k) \\ y(k) = C_m x(k) \end{cases}. \tag{4}$$

Define $\bar{x}(k) = \begin{bmatrix} x(k) & f_a(k) \end{bmatrix}^T$. Based on Equation (4), the following discrete-time system equation for the expanded system can be derived:

$$\begin{cases} \bar{x}(k+1) = \bar{A}\bar{x}(k) + \bar{B}u(k) + H(k) \\ y(k) = \bar{C}_m \bar{x} \end{cases}, \tag{5}$$

where $\bar{A} = \begin{bmatrix} \Phi & \Gamma_a \\ 0 & 1 \end{bmatrix}$, $\bar{B} = \begin{bmatrix} \Gamma \\ 0 \end{bmatrix}$, $\bar{C}_m = \begin{bmatrix} C_m & 0 \end{bmatrix}$, $H(k) = \begin{bmatrix} 0 & \triangle h \end{bmatrix}^T$, $\triangle h = f_a(k+1) - f_a(k)$.

2.2. Design and Analysis of N-Step Extended State Observer

Considering the engine system described by Equation (5), which incorporates actuator faults, the one-step extended state fault-tolerant observer is designed as follows:

$$\begin{cases} z_{x1}(k+1) = \Phi z_{x1}(k) + \Gamma u(k) \\ \qquad\qquad + K_1(y(k) - Cmz_{x1}(k)) \\ z_{f_{a1}}(k+1) = z_{f_{a1}}(k) + K_2(y(k) - Cmz_{x1}(k)) \end{cases}, \tag{6}$$

where z_{x1} represents the state of the one-step observer, $z_{f_{a1}}$ denotes the first estimate of $f_a(k)$, and K_1 and K_2 represent the observer gains. Furthermore, Equation (6) can be expressed in the following expanded form as a state observer:

$$\begin{cases} z_1(k+1) = \bar{A}z_1(k) + \bar{B}u(k) + L(y(k) - \bar{C}_m z_1(k)) \\ \hat{y}_1(k) = \bar{C}_m z_1(k) \end{cases}. \tag{7}$$

Define $e_{x1}(k) = x(k) - z_{x1}(k)$, $e_{f_{a1}}(k) = f_a(k) - z_{f_{a1}}(k)$, and $e_1(k) = \begin{bmatrix} e_{x1}(k) & e_{f_{a1}}(k) \end{bmatrix}^T$.

Based on system (7) and system (5), the error estimation system can be constructed as follows:

$$\begin{cases} e_1(k+1) = (\bar{A} - L\bar{C}_m)e_1(k) + I_1 \\ e_{y1}(k) = \bar{C}_m e_1(k) \end{cases}, \tag{8}$$

where $I_1 = H(k)$.

To enhance the estimation accuracy of the observer, the two-step extended state fault-tolerant observer for system (5), building upon the one-step observer, is designed as follows:

$$\begin{cases} z_{x2}(k+1) = \Phi z_{x2}(k) + \Gamma u(k) \\ \qquad\qquad +K_1(y(k) - C_m z_{x2}(k)) \\ z_{f_{a2}}(k+1) = z_{f_{a2}}(k) + K_2(y(k) - C_m z_{x2}(k)) \\ \qquad\qquad + \triangle z_{f_{a1}}(k+1) \end{cases}, \tag{9}$$

where z_{x2} represents the state of the two-step observer, $z_{f_{a2}}$ denotes the second estimate of $f_a(k)$, and K_1 and K_2 represent the observer gains. Furthermore, Equation (9) can be expressed in the following expanded form as a state observer:

$$\begin{cases} z_2(k+1) = \bar{A} z_2(k) + \bar{B} u(k) + L(y(k) - \bar{C}_m z_2(k)) \\ \hat{y}_2(k) = \bar{C}_m z_2(k) \end{cases} \tag{10}$$

Define $e_{x2}(k) = x(k) - z_{x2}(k)$, $e_{f_{a2}}(k) = f_a(k) - z_{f_{a2}}(k)$, $e_2(k) = \begin{bmatrix} e_{x2}(k) & e_{f_{a2}}(k) \end{bmatrix}^T$.

Based on systems (5) and (10) , the error estimation system can be constructed as follows:

$$\begin{cases} e_2(k+1) = (\bar{A} - L\bar{C}_m) e_2(k) + I_2 \\ e_{y2}(k) = \bar{C}_m e_2(k) \end{cases}, \tag{11}$$

where $I_2 = \begin{bmatrix} 0 & \Delta h - \Delta z_{f_{a1}}(k) \end{bmatrix}^T$.

The n-step extended state fault-tolerant observer is designed as follows:

$$\begin{cases} z_{xn}(k+1) \;\; = \Phi z_{xn}(k) + \Gamma u(k) \\ \qquad\qquad +K_1(y(k) - C_m z_{xn}(k)) \\ z_{f_{a(n)}}(k+1) = z_{f_{a(n)}}(k) + K_2(y(k) - C_m z_{xn}(k)) \\ \qquad\qquad + \triangle z_{f_{a(n-1)}}(k+1) \end{cases}, \tag{12}$$

where z_{xn} represents the state of the n-step observer, $z_{f_{a(n)}}(k)$ denotes the n-step estimate of $f_a(k)$, and K_1 and K_2 represent the observer gains. Furthermore, Equation (12) can be expressed in the following expanded form as a state observer:

$$\begin{cases} z_n(k+1) = \bar{A} z_n(k) + \bar{B} u(k) + L(y(k) - \bar{C}_m z_n(k)) \\ \hat{y}_n(k) = \bar{C}_m z_n(k) \end{cases}. \tag{13}$$

Similar to the two-step observer, the error estimation based on the original state (5) and (13) can be established as follows:

$$\begin{cases} e_n(k+1) = (\bar{A} - L\bar{C}_m) e_n(k) + I_n \\ e_{yn}(k) = \bar{C}_m e_n(k) \end{cases}, \tag{14}$$

where $I_n = \begin{bmatrix} 0 & \Delta h - \Delta z_{f_{a(n-1)}}(k) \end{bmatrix}^T$.

Theorem 1. *Define $\bar{A} - L\bar{C}_m = \Psi$. If Ψ is a Hurwitz matrix, the state error predicted by the n-step extended state fault-tolerant controller is bounded.*

Proof. The Lyapunov function is selected as $V(e_n(k)) = e_n^T(k) U e_n(k)$, where the matrix U is the unique solution of the Lyapunov equation $\Psi^T U \Psi - U = -V$, with $U > 0$ and $V > 0$ being symmetric matrices.

$$\begin{aligned} \triangle V(e_n(k+1)) &= V(e_n(k+1)) - V(e_n(k)) \\ &= (\Psi e_n(k) + I_n(k))^T U (\Psi e_n(k) + I_n(k)) \\ &- e_n(k)^T U e_n(k) \\ &= -e_n(k)^T V e_n(k) + 2 I_n(k)^T U \Psi e_n(k)) \\ &+ I_n^T(k) U I_n(k). \end{aligned} \tag{15}$$

Let $R(k) = e_n(k) V^{1/2}$, $S(k) = I_n^T(k) U \Psi V^{-1/2}$, $M(k) = I_n^T(k) U^{1/2}$, then we have:

$$\begin{aligned} \triangle V(e_n(k+1)) = &- \parallel R(k) - S(k) \parallel_2^2 \\ &+ \parallel S(k) \parallel_2^2 + \parallel M(k) \parallel_2^2, \end{aligned} \tag{16}$$

if $\| e_n(k) \|_2 > \| I_n^T(k)U\Psi \|_2 + (\| I_n^T(k)U\Psi \|_2^2 + \| I_n(k)U^{1/2} \|_2^2)$, and $V = I$, then $\| R(k) \|_2 > \| S(k) \|_2 + (\| S(k) \|_2^2 + \| R(k) \|_2^2)^{1/2}$, and since $\| R(k) - S(k) \|_2 > \| R(k) \|_2 - \| S(k) \|_2$, it follows that $\| R(k) - S(k) \|_2^2 > \| S(k) \|_2^2 + \| M(k) \|_2^2$. Thus, it can be shown that $\triangle V(e_n(k+1)) < 0$. This implies that $e_n(k)$ is decreasing , and consequently $e_n(k)$ is bounded. □

2.3. Design of the MPC Fault-Tolerant Controller

The predictive fault-tolerant control method proposed in this study exhibits fundamental differences from conventional state-observer-based approaches: while traditional methods require additional compensation control law design after fault observation, our solution employs an n-step extended state observer to estimate fault signals in real-time and online updates predictive model parameters, achieving adaptive reconfiguration of the control law. This integrated design not only eliminates the need for designing separate compensation controllers as in conventional methods, but more importantly unifies fault suppression and performance optimization within the model predictive control framework.

By utilizing the n-step extended state observer, an accurate engine model incorporating actuator faults is derived. The sequential application of model predictive control allows the engine system to operate optimally while adhering to safety constraints. Instead of relying on the actual system model, Equation (13) is employed. The structure of the entire system is illustrated in Figure 1.

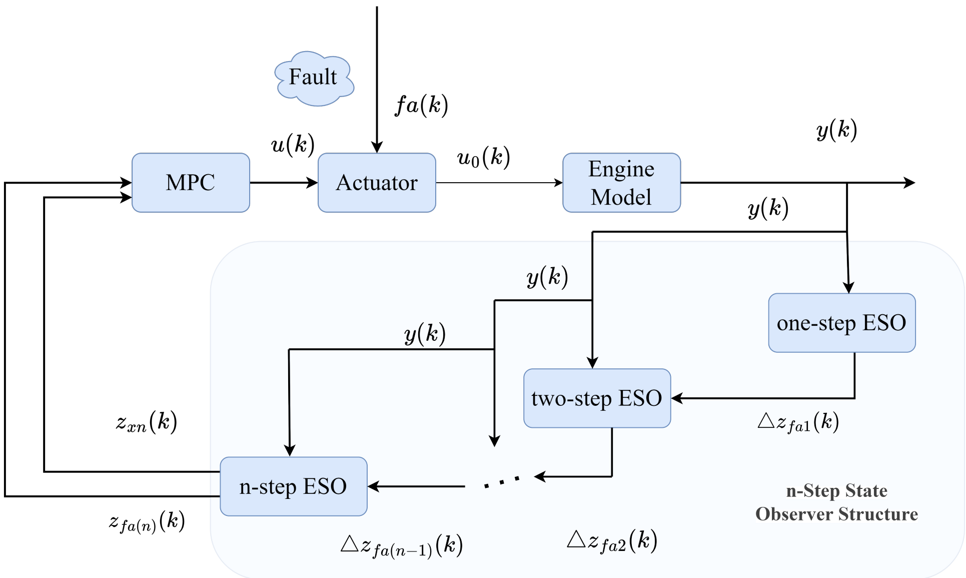

Figure 1. Model predictive controller structure based on n-step observer.

Compared to the actual model, the observer model integrates estimated actuator faults. As a result, the system described by Equation (13) closely approximates the real-time online engine model after n–step observation, effectively addressing system instability caused by actuator faults. Furthermore, by performing rolling optimization within the model prediction framework, the current optimal inputs are predicted while explicitly incorporating actuator fault signals.

Without loss of generality, the control objective is defined as $x \to x_o$, where x_o represents the desired low-pressure speed change. Therefore, the cost function J is defined as:

$$\begin{aligned} \min J = \textstyle\sum_{i=1}^{N} \{ & \| z_{nL}(k+i) - x_0(k+i) \|_P^2 \\ & + \| u(k) \|_Q^2 \} \end{aligned}, \tag{17}$$

where N is the prediction horizon, $P > 0$, $Q > 0$ are the weight matrix.

From the prediction model (13) equation, the predicted low-pressure rotational speed increment $\hat{x}_{nH}$ can be obtained as follows:

$$\hat{X}_{nL}(k) = Ez_n(k) + Fu(k-1) + G\triangle\hat{U}(k) + S_f, \tag{18}$$

where $S_f = \begin{bmatrix} C_{zx}A_f \\ C_{zx}(\bar{A}A_f + A_f) \\ \vdots \\ C_{zx}\sum_{i=0}^{N-1}\bar{A}^i A_f \end{bmatrix}$, $A_f = L(y(k) - \bar{C}_m z_n(k))$.

The performance index function (17) of the aircraft engine control system is derived as follows:

$$\begin{aligned} minJ &= \| X_0(k) - \hat{X}_{nL} \|_P^2 + \| \triangle\hat{U}(k) \|_Q^2 \\ &= (X_0(k) - \hat{X}_{nL})^T \tilde{P}(X_0(k) - \hat{X}_{nL}) \\ &+ \triangle\hat{U}(k)^T \tilde{Q}\triangle\hat{U}(k) \\ &= X_0(k)^T \tilde{P} X_0(k) - 2X_0(k)^T \tilde{P}\hat{X}_{nL}(k) \\ &+ \hat{X}_{nL}(k)^T \tilde{P}\hat{X}_{nL}(k) + \triangle\hat{U}(k)^T \tilde{Q}\triangle\hat{U}(k) \end{aligned} . \tag{19}$$

Bringing (18) into (19) yields $minJ = \triangle\hat{U}(k)^T(G^T\tilde{P}G+\tilde{Q})\triangle\hat{U}(k)+(2z_n(k)^T E^T\tilde{P}G+2u(k-1)F^T\tilde{P}G-2\hat{X}_{nL}(k)\tilde{P}G + 2S_f\tilde{P}G)\triangle\hat{U}(k) + const.$

where $\tilde{P} = \begin{bmatrix} P & 0 & \cdots & 0 \\ 0 & P & \cdots & 0 \\ \vdots & \vdots & \ddots & \vdots \\ 0 & 0 & \cdots & P \end{bmatrix}$, $\tilde{Q} = \begin{bmatrix} Q & 0 & \cdots & 0 \\ 0 & Q & \cdots & 0 \\ \vdots & \vdots & \ddots & \vdots \\ 0 & 0 & \cdots & Q \end{bmatrix}$, $const$ denotes a constant.

The above optimization problem can be transformed into the following form for solution:

$$minJ = 1/2\triangle\hat{U}(k)^T\Theta\triangle\hat{U}(k) + T\triangle\hat{U}(k), \tag{20}$$

where $\Theta = 2(G^T\tilde{P}G + \tilde{Q}), T = 2z_n(k)^T E^T\tilde{P}G + 2u(k-1)^T F^T\tilde{P}G - 2\hat{X}_{nL}(k) + 2S_f^T\tilde{P}$.

System constraints are incorporated into the performance metrics, with particular emphasis on fuel variation and the rate of fuel variation. The constraints are defined as follows:

$$\triangle u_{min} \leq \triangle\hat{u}(k+j \mid k) \leq \triangle u_{max}$$

$$u_{min} \leq \hat{u}(k+j \mid k) \leq u_{max}$$

The above constraints can be transformed into a matrix form as follows:

$$\begin{bmatrix} M_1 \\ M_2 \end{bmatrix}\triangle\hat{U}(k) \leq \begin{bmatrix} m_1 \\ m_2 \end{bmatrix}$$

$$m_1 = \begin{bmatrix} \triangle u_{max} & \ldots & \triangle u_{max} & -\triangle u_{min} & \cdots & -\triangle u_{min} \end{bmatrix}^T$$

$$\begin{aligned} m_2 = [&u_{max} - u(k-1) \ \cdots \ u_{max} - u(k-1) \\ &-u_{min} + u(k-1) \ \cdots \ -u_{min} + u(k-1)]^T \end{aligned}$$

The above optimization problem can thus be transformed into a standard quadratic programming problem and thus solved:

$$\begin{cases} \min J = \dfrac{1}{2}\triangle\hat{U}(k)^T\Theta\triangle\hat{U}(k) + T\triangle\hat{U}(k), \\ \text{s.t.} \quad \begin{bmatrix} M_1 \\ M_2 \end{bmatrix}\triangle\hat{U}(k) \leq \begin{bmatrix} m_1 \\ m_2 \end{bmatrix}. \end{cases} \tag{21}$$

The optimal inputs for achieving the desired engine speed under actuator fault conditions are determined through Algorithm 1, which is developed based on the proposed n-step extended state observer and model predictive control framework. The algorithm systematically outlines the necessary steps to ensure accurate and efficient control performance.

Algorithm 1 MPC based on n-step observer structure

1: Set the initial sampling time $k = 1$,initialize the system's estimated state $z_1(1) \dots z_n(1)$, and input $u(0)$
2: **While** system state has not reached setpoint, **do**
3: Compute next-step state estimates for each observer sequentially using Equation (13)
4: Solve the problem (20) to obtain the optimal input $\triangle\hat{U}^*(k)$
5: Take $\triangle u^*(k)$ in $\triangle\hat{U}^*(k)$ to obtain $u^*(k+1)$, and then take $u^*(k+1)$ into Equation (4)
6: Measure current output $y(k+1)$
7: Update state estimates by substituting $u^*(k+1)$, $y(k+1)$ into observer Equation (13)
8: $k = k+1$
9: **end**

2.4. Stability Analysis

Theorem 2. *The engine system is stabilized against continuous fault signals through the integration of K_x into MPC , as formulated in Equation (21), in conjunction with ESO gain L , which is derived in Theorem 1. This approach ensures robust stability and effective fault tolerance within the control framework.*

Proof. Define K_X as the input gain obtained from the model predictive controller solution. By combining Equations (13) and (14), and the control law, the engine system is given by:

$$\tilde{x}(k+1) = \tilde{A}\tilde{x}(k) + \tilde{B}\nu(k), \tag{22}$$

where,
$$\tilde{x}(k) = \begin{bmatrix} x(k+1) \\ \\ e_n(k+1) \end{bmatrix}, \nu(k) = \begin{bmatrix} In(k) \\ \\ f_a(k) \end{bmatrix}, \tilde{A} = \begin{bmatrix} A + BK_x & B\bar{K} \\ 0 & \Psi \end{bmatrix}, \tilde{B} = \begin{bmatrix} 0 & \Gamma_a \\ I & 0 \end{bmatrix}, \overline{K} = [K_x, 0]. \qquad \square$$

For the above system, the Lyapunov function in the form of Equation (23) is chosen as follows:

$$V(x(k), e_n(k)) = x(k)^T P x(k) + \gamma e_n(k)^T Q e_n(k), \tag{23}$$

where, γ is a regulation parameter, usually used for the performance or stability of a control system.

Define $\triangle V(x(k+1), e_n(k+1)) = V(x(k+1), e_n(k+1)) - V(x(k), e_n(k))$, then

$$\begin{aligned} &\triangle V(x(k+1), e_n(k+1)) \\ &= x^T(k+1)Px(k+1) + \gamma e_n^T(k+1)Qe_n(k+1) \\ &\quad - x^T(k)Px(k) - \gamma e_n^T(k)Qe_n(k). \end{aligned} \tag{24}$$

Substituting Equation (22) into the above equation yields:

$$\begin{bmatrix} x(k) \\ f_a(k) \\ e_n(k) \end{bmatrix}^T \Lambda_1 \begin{bmatrix} x(k) \\ f_a(k) \\ e_n(k) \end{bmatrix} \leq 0, \tag{25}$$

where,

$$\Lambda_1 = \begin{bmatrix} A_f^T P A_f - P & * & * \\ \Gamma_a^T P A_f & \Gamma_a^T P \Gamma_a & * \\ \overline{K}^T B^T P A_f & \overline{K}^T B^T P \Gamma_a & \overline{K}^T B^T P B \overline{K} - \gamma\psi \end{bmatrix},$$
$$\psi = Q - \Psi^T Q \Psi, A_f = A + BK_x.$$

Let $y \in \Omega$, and suppose there exist a matrix G and a scalar g such that the ellipsoid $\sigma = \{y(k) \mid Gy(k) + g \leq 1\}$ serves as an external approximation of the set Ω.

It can be rewritten as:

$$(Gy + g)^T(Gy + g) \leq 1. \tag{26}$$

Rewriting the above equation in matrix form, we obtain:

$$\begin{bmatrix} y(k) \\ 1 \end{bmatrix}^T \Lambda_2 \begin{bmatrix} y(k) \\ 1 \end{bmatrix} \leq 0, \tag{27}$$

where, $\Lambda_2 = \begin{bmatrix} G^TG & * \\ g^TG & g^Tg - 1 \end{bmatrix}$.

Combining Equations (25) and (27), we obtain:

$$\begin{bmatrix} x(k) \\ f_a(k) \\ e_n(k) \end{bmatrix}^T \Lambda_1 \begin{bmatrix} x(k) \\ f_a(k) \\ e_n(k) \end{bmatrix} - \lambda \begin{bmatrix} y(k) \\ 1 \end{bmatrix}^T \Lambda_2 \begin{bmatrix} y(k) \\ 1 \end{bmatrix} \leq 0, \tag{28}$$

when $y(k) = C_m x(k)$ is substituted into Equation (28) yields:

$$\begin{bmatrix} x(k) \\ f_a(k) \\ e_n(k) \\ 1 \end{bmatrix}^T \Lambda_3 \begin{bmatrix} x(k) \\ f_a(k) \\ e_n(k) \\ 1 \end{bmatrix} - \begin{bmatrix} x(k) \\ f_a(k) \\ e_n(k) \\ 1 \end{bmatrix}^T \Lambda_4 \begin{bmatrix} x(k) \\ f_a(k) \\ e_n(k) \\ 1 \end{bmatrix} \leq 0, \tag{29}$$

where, $\Lambda_3 = \begin{bmatrix} \Lambda 1 \\ 0 \end{bmatrix}$,

$$\Lambda 4 = \begin{bmatrix} C_m^TG^TGC_m & * & * & * \\ 0 & 0 & * & * \\ 0 & 0 & 0 & * \\ f^TGC_m & 0 & 0 & g^Tg - 1 \end{bmatrix}.$$

Organizing the above equation yields:

$$\begin{bmatrix} A_1 & A_2^T \\ A_2 & A_3 \end{bmatrix} \leq 0, \tag{30}$$

where,

$$A1 = \begin{bmatrix} \theta & * & * \\ \Gamma_a^T P A_f & \Gamma_a^T P \Gamma_a & * \\ \overline{K}^T B^T P A_f & \overline{K}^T B^T P \Gamma_a & \overline{K}^T B^T P B \overline{K} - \gamma\psi \end{bmatrix},$$

$$\theta = A_f^T P A_f - P - \lambda C_m^T G^T G C_m,\ A2 = \begin{bmatrix} -\lambda g^T G C_M & 0 & 0 & -\lambda g^T g + \lambda \end{bmatrix},\ A_3 = -\lambda g^T g + \lambda.$$

Rewriting the above equation in the following form:

$$\Lambda_5 - \begin{bmatrix} A_f^T \\ \Gamma_a^T \\ \bar{K} B^T \\ 0 \end{bmatrix} P \begin{bmatrix} A_f & B\bar{K} & \Gamma_a & 0 \end{bmatrix} \geq 0, \tag{31}$$

where, $\Lambda_5 = \begin{bmatrix} P + \lambda C_m^T G^T G C_m & * & * & * \\ 0 & 0 & * & * \\ 0 & 0 & \gamma\psi & * \\ \lambda g^T G C_M & 0 & 0 & \lambda g^T g - \lambda \end{bmatrix}$.

Using the Schur complement,we can obtain:

$$\begin{bmatrix} P+\lambda C_m^T G^T G C_m & * & * & * & * \\ 0 & 0 & * & * & * \\ 0 & 0 & \gamma\psi & 0 & * \\ \lambda g^T GC & 0 & 0 & \lambda g^T g-\lambda & * \\ A_f & B_d & B\bar{K} & 0 & P^{-1} \end{bmatrix}. \tag{32}$$

Here, we adopt the approach taken in the literature [25], and multiply both sides of the equation by

$$\mu = \begin{bmatrix} I & 0 & 0 & 0 & 0 \\ 0 & 0 & 0 & I & 0 \\ 0 & 0 & 0 & 0 & I \\ 0 & I & 0 & 0 & 0 \\ 0 & 0 & I & 0 & 0 \end{bmatrix}$$

and μ^T, respectively.

$$\begin{bmatrix} \Xi & * \\ O & \gamma\varpi \end{bmatrix} \geq 0, \tag{33}$$

where,

$$\Xi = \begin{bmatrix} P+\lambda C_m^T G^T G C_m & * & * \\ \lambda g^T G C_m & \lambda(g^T g-1) & * \\ A_f & 0 & P^{-1} \end{bmatrix} > 0,$$

$$O = \begin{bmatrix} 0 & 0 & \Gamma_a^T \\ 0 & 0 & \overline{K}^T B^T \end{bmatrix},$$

$$\varpi = \begin{bmatrix} 0 & 0 \\ 0 & \psi \end{bmatrix}.$$

If γ is large enough, by utilizing the Schur complement, we have $\gamma\varpi - O\Xi^{-1}O^T > 0$, thus proving the stability of the system.

3. Simulation and Experiments

In this paper, the numerical model$n_L = 96\% n_{Lmax}$, which is commonly used in aero-engine control, is selected. This model is established based on the power extraction method, with detailed steps following the standard modeling procedure. The resulting numerical model is given as follows:

$$A = \begin{bmatrix} -2.322 & -0.509 \\ 3.5 & -5.98 \end{bmatrix}, B = \begin{bmatrix} 8460 \\ 9974 \end{bmatrix}, C_m = \begin{bmatrix} 1 & 0 \end{bmatrix}, C = \begin{bmatrix} -798 & -940.9 \end{bmatrix}^T.$$

Set the sampling period T =0.005 s, the actuator fault signal is set to $5sin10t$, and then discretize the system to get the initial state of the system where the engine's low and low voltage speed variations $x(2) = \begin{bmatrix} -300 & -348 \end{bmatrix}^T$, the control constraints are: the rate of change of fuel quantity, $\frac{\triangle u(k)}{T} \leq$ 0.05 kg/s, the maximum change of fuel quantity $\triangle u_{max} =$ 0.6 kg, and the control objective is to make the change of low-pressure speed $\triangle n_H =$ 0 r/min. The observation gain matrix of the ESO $L = \begin{bmatrix} 1.5 & 1.5 & -0.1 \end{bmatrix}^T$ is selected based on Theorem 1 , where the prediction step in the model predictive control is N =5, and the corresponding weighting matrix is $Q =$ 0.1 and $R =$ 1, set the sampling time $T_s =$ 2.5 s. The proposed n-step observer's effectiveness is validated by comparing one-step and three-step observer performance (Figures 2 and 3). Results show the three-step observer achieves significantly better fault signal estimation accuracy than the one-step observer, demonstrating the method's enhanced precision. The observer's flexibility allows optimal step selection (n) based on system requirements for improved fault estimation.

As illustrated in Figure 4, the integration of the one-step observer with the model predictive controller is found to produce significant estimation errors, resulting in a misalignment between the observer model and the actual system dynamics. This misalignment leads to failure in the rolling optimization process of the model predictive control framework to generate an effective control response. Consequently, substantial fluctuations in the low-pressure rotor speed are observed, preventing convergence to the desired set point. In contrast, Figure 5 reveals that the proposed n-step observer enables the system to achieve and maintain the target rotational speed without the oscillations observed in the one-step observer scenario. This improvement underscores the superior predictive capability of the n-step observer, which not only enhances estimation accuracy but also supports the rolling optimization process in generating optimal control inputs that comply with system constraints. Consequently, the proposed approach significantly improves the system's fault tolerance and overall control performance.

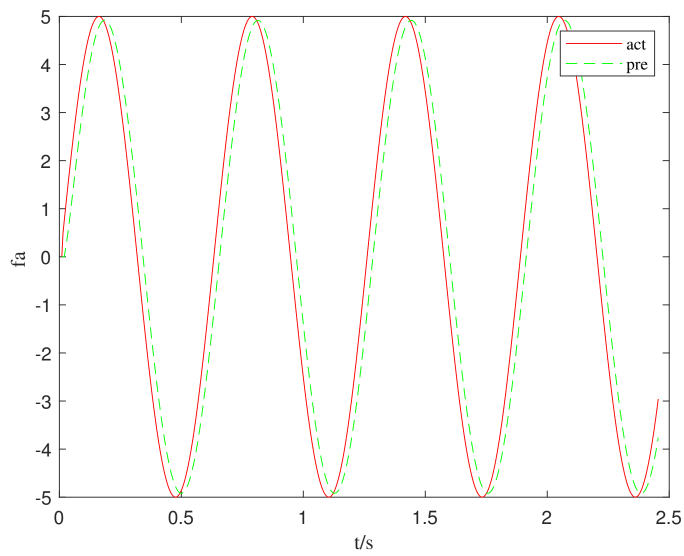

Figure 2. Estimated and actual fault signal under of a one-step observer.

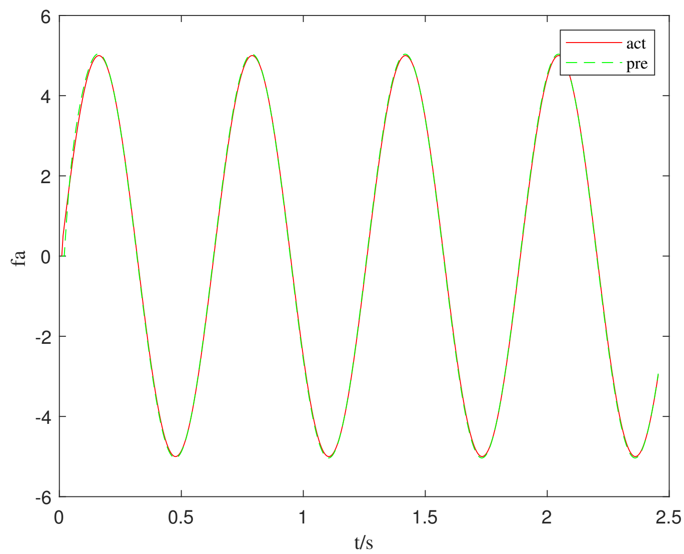

Figure 3. Estimated and actual fault signal under of a three-step observer.

As shown in Figure 6, when the model predictive control is implemented with the three-step observer, the estimation error between the observer and the actual system state is reduced as the number of observer steps increases. This demonstrates that the three-step observer provides a more accurate representation of the system dynamics compared to the one-step observer, thereby enhancing the predictive accuracy of the control process. In practical applications, the number of observer steps can be tailored to meet the specific control performance requirements of the system. By optimizing the number of steps, the estimation accuracy of the observer is improved, leading to enhanced control effectiveness and overall system stability.

Furthermore, as depicted in Figure 7, the model predictive controller utilized in this study reveals that an extended prediction horizon leads to a slower response of the engine system. Although a longer prediction horizon enhances the controller's capability to predict future system behavior, it also substantially increases computational complexity. Therefore, the selection of an appropriate prediction horizon necessitates a trade-off between control performance and computational efficiency, ensuring that the system achieves its specific performance requirements while maintaining real-time feasibility.

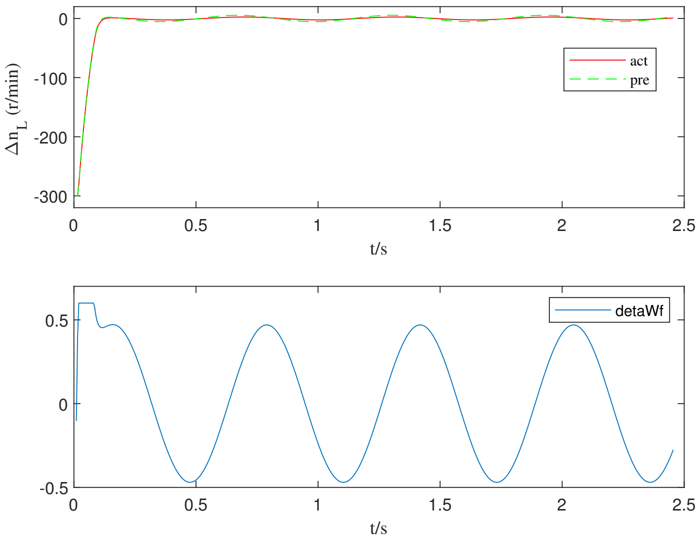

Figure 4. Changes in the response of the system under MPC control based on a one-step observer.

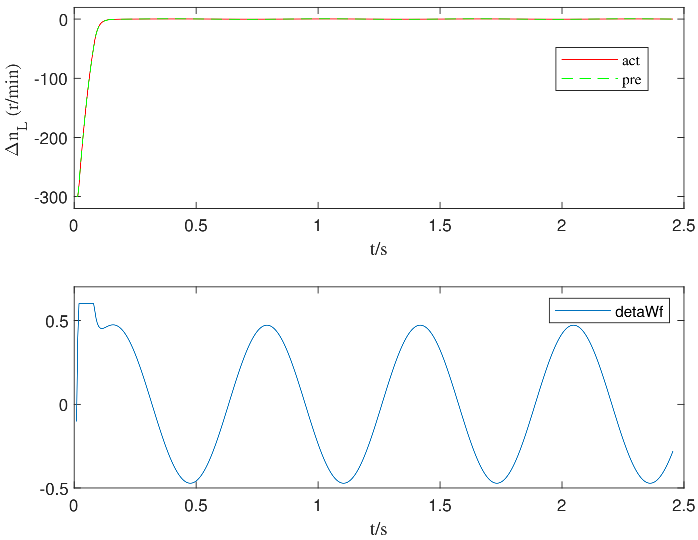

Figure 5. Changes in the response of the system under MPC control based on a three-step observer.

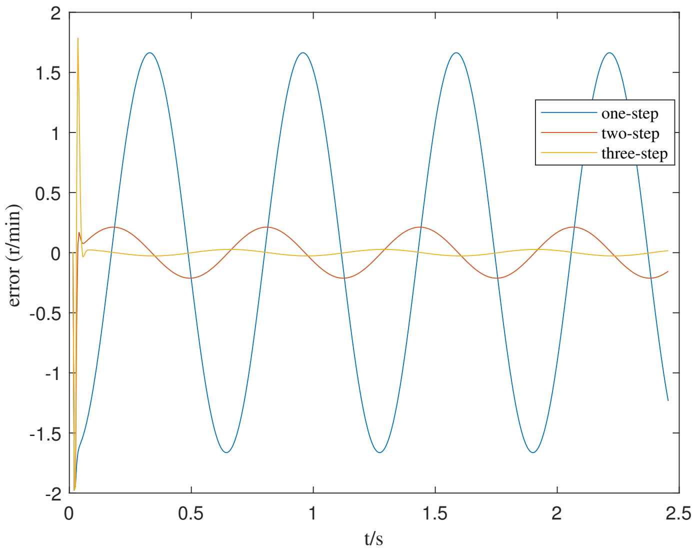

Figure 6. Error between the state observed by each step observer and the true state.

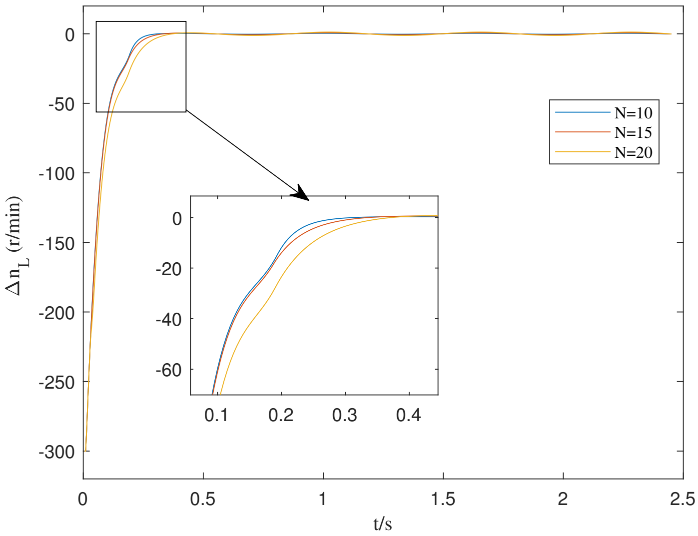

Figure 7. low voltage rotor speed variation with varying prediction horizon.

Additionally, to validate the applicability of the proposed method in predicting continuous fault signals, a peak-like fault signal is introduced, as illustrated in Figure 8. This scenario is designed to evaluate the observer's capability to accurately estimate abrupt fault variations and to assess its effectiveness in real-time fault prediction and compensation within the control framework.

The aforementioned fault signals are applied to the engine system, with both one-step and three-step extended state observer configurations being employed for fault signal estimation. The corresponding results are presented in Figures 9 and 10. As clearly demonstrated in these figures, although the one-step observer successfully predicts the fault signal, its estimation accuracy is markedly inferior to that achieved by the three-step observer configuration. This observation underscores the improved fault prediction performance of the three-step observer, demonstrating its superior ability to provide more accurate fault estimations.

The dynamic response of the engine low-pressure spool speed in Figures 11 and 12 shows that the predictive controller drives the rotor to converge to the steady-state operating point while satisfying all constraints. In the presence of an actuator fault, the observer initiates the estimation of fault signals. A comparative analysis between predictive control using the one-step and three-step observers reveals that the rotational speed fluctuation at the steady-state operating point is significantly larger when the one-step observer is employed. Furthermore, the fluctuation at the peak of the fault signal is approximately twice as large in the one-step observer compared to the three-step observer. These findings demonstrate the enhanced fault tolerance and more stable performance of the three-step observer in managing actuator faults.

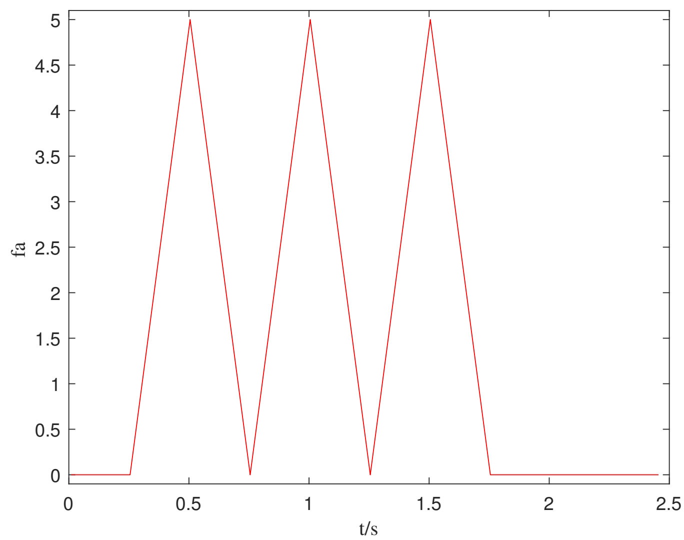

Figure 8. A peak-like fault signal.

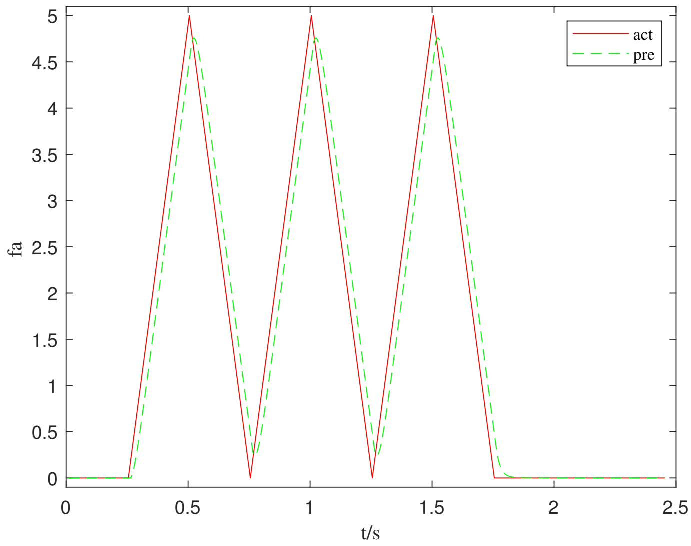

Figure 9. Estimated and actual fault signal under of a one-step observer.

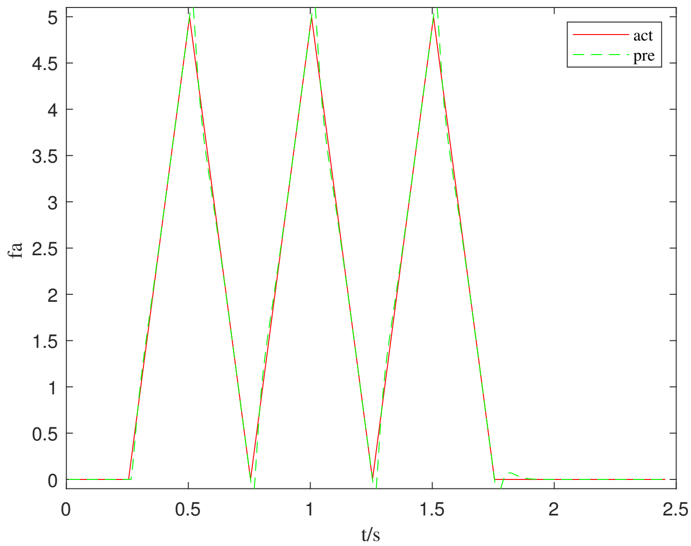

Figure 10. Estimated and actual fault signal under of a three-step observer.

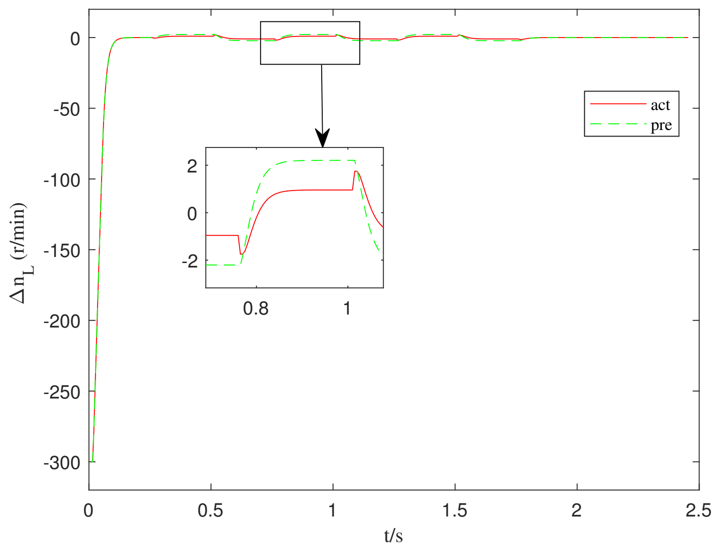

Figure 11. Dynamic response of the system under one-step observer-based control.

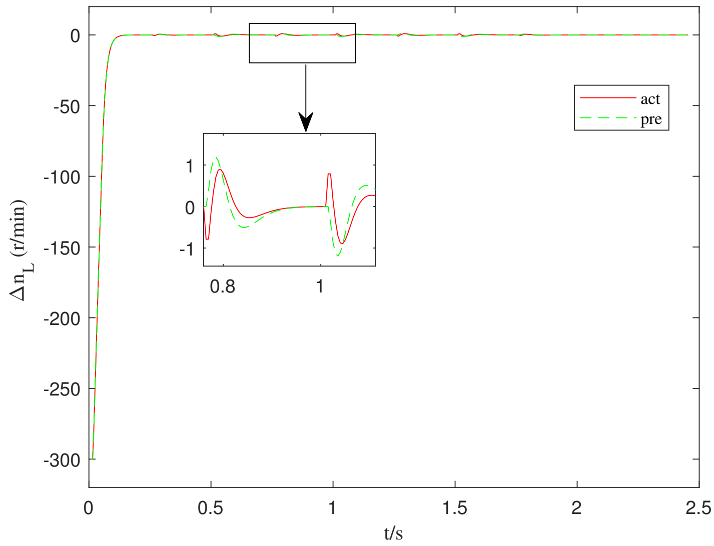

Figure 12. Dynamic response of the system under three-step observer-based control.

4. Conclusions

This study proposes an n-step extended state observer, which achieves lower observation accuracy compared to conventional extended state observers. Furthermore, unlike traditional feedback controllers that often disregard system constraints, this work integrates model predictive control and incorporates the estimated fault signals into the predictive model, thereby significantly enhancing control performance. The proposed MPC framework, based on the n-step extended state observer, is validated through simulations, which demonstrate its effectiveness in addressing actuator faults and optimizing system performance. The results underscore the advantages of the n-step observer in delivering more accurate fault predictions, resulting in improved fault tolerance and stability in the engine control system.

Author Contributions

Y.L.: methodology, writing—original draft preparation; S.L.: methodology, data curation; N.X.: supervision; X.Z.: writing—reviewing and editing. All authors have read and agreed to the published version of the manuscript.

Funding

This work was supported by National Science and Technology Major Project (J2019-V-0010-0105).

Data Availability Statement

The authors confirm that the data supporting the findings of this study are available within the article.

Acknowledgments

The authors gratefully acknowledge anonymous editors and reviewers.

Conflicts of Interest

The authors declare no conflict of interest.

References

1. Fu, S.; Tang, W.; Wang, R.; et al. Actuator Fault-Tolerant Control for Aero-Engine Control System: A Zonotope-Based Approach. *IEEE Trans. Intell. Transp. Syst.* **2024**, *25*, 18861–18871.
2. Al Seiari, S.; Cen, Z.; Youssef, H.; et al. Aeroengine Actuator Fault Detection and Estimation Via Combined Model Observers. *IFAC-PapersOnLine* **2024**, *58*, 121–125
3. Du, X.; Zhao, Y.; Sun, X. Bumpless Switching Control for Aircraft Engine Control Systems with Actuator Fault Based on Switched LPV Models. *IEEE Trans. Ind. Electron.* **2024**, *72*, 4127–4136.
4. Wang, H.; Daley, S. Actuator fault diagnosis: An adaptive observer-based technique. *IEEE Trans. Autom. Control* **1996**, *41*, 1073–1078

5. Zhang, A.; Hu, Q.; Zhang, Y. Observer-Based Attitude Control for Satellite Under Actuator Fault. *J. Guid. Control Dyn.* **2015**, *38*, 4.
6. Song, G. Design of a novel switched fault estimator with adaption law for non-linear switched systems and application to chemical systems. *Multiscale Multidiscip. Model. Exp. Des.* **2024**, *7*, 4189–4202.
7. Chen, B.-S.; Liu, H.-T.; Wu, R.-S. Robust H_∞ Fault-Tolerant Observer-Based PID Path Tracking Control of Autonomous Ground Vehicle with Control *Saturation. IEEE Open J. Veh. Technol.* **2024**, *5*, 298–311.
8. Huang, M.; Ding, L.; Li, W.; et al. Distributed Observer-Based H_∞ Fault-Tolerant Control for DC Microgrids with Sensor Fault. *IEEE Trans. Circuits Syst. I Regul. Pap.* **2021**, *68*, 1659–1670.
9. Adamczyk.; Michal. ; Orlowska-Kowalska.; Teresa. Self-correcting virtual current sensor based on the modified Luenberger observer for fault-tolerant induction motor drive.*Energies* **2021**,*14*,6767.
10. Lee, J.D.; Im, S.; Kim, L.; et al. Data-Driven Fault Detection and Isolation for Multirotor System Using Koopman Operator. *J. Intell. Robot. Syst.* **2024**, *110*, 128.
11. Yang, W.; Dong, J. Distributed Adaptive Observer-Based Fault-Tolerant Output Consensus for Heterogeneous MASs. *IEEE Trans. Syst. Man Cybern. Syst.* **2024**, *54*, 2414–2425.
12. Van, M.; Mavrovouniotis, M.; Ge, S.S. An Adaptive Backstepping Nonsingular Fast Terminal Sliding Mode Control for Robust Fault Tolerant Control of Robot Manipulators. *IEEE Trans. Syst. Man Cybern. Syst.* **2019**, *49*, 1448–1458.
13. Wang, L.; Yuan, D.; Cao, R.; et al. Automatic landing of carrier-based aircraft based on a collaboration of fault reconstruction and fault-tolerant control. *Aerosp. Sci. Technol.* **2024**, *144*, 108772.
14. Zhang, Y.; Han, W. Extended Observer-Based Fault-Tolerant Attitude Control of Hypersonic Reentry Vehicle Considering Actuator and Sensor Faults. In Proceedings of the 2024 6th International Conference on Electronic Engineering and Informatics (EEI), Chongqing, China, 28–30 June 2024; pp. 307–312.
15. Wang, K.; Meng, T.; Wang, W.; et al. Finite-time extended state observer based prescribed performance fault tolerance control for spacecraft proximity operations. *Adv. Space Res.* **2022**, *70*, 1270–1284.
16. Huang, S.-J.; Yang, G.-H. Fault Tolerant Controller Design for T-S Fuzzy Systems with Time-Varying Delay and Actuator Faults: A K-Step Fault-Estimation Approach. *IEEE Trans. Fuzzy Syst.* **2014**, *22*, 1526–1540.
17. Qi, G.; Hu, J.; Li, L.; et al. Integral Compensation Function Observer and Its Application to Disturbance-Rejection Control of QUAV Attitude. *IEEE Trans. Cybern.* **2024**, *54*, 4088–4099.
18. Li, X.; Ahn, C.K.; Lu, D.; et al. Robust Simultaneous Fault Estimation and Nonfragile Output Feedback Fault-Tolerant Control for Markovian Jump Systems. *IEEE Trans. Syst. Man Cybern. Syst*. **2019**, *49*, 1769–1776.
19. Du, Y.; Jiang, B.; Ma, Y. Adaptive optimal sliding-mode fault-tolerant control for nonlinear systems with disturbances and estimation errors. *Complex Intell. Syst.* **2023**, *10*, 1087–1101.
20. Zhao, X.; Meng, B.; Wang, Z. Fault-tolerant adaptive event-triggered integral sliding mode control for uncertain networked systems under actuator failures. *J. Frankl. Inst.* **2024**, *361*, 1544–1554.
21. Zhang, H.; Zhu, D.; Liu, C.; et al. Tracking fault-tolerant control based on model predictive control for human occupied vehicle in three-dimensional underwater workspace. *Ocean. Eng.* **2022**, *249*, 110845.
22. Shi, H.; Zuo, L.; Wang, S.; et al. Robust predictive fault-tolerant switching control for discrete linear systems with actuator random failures. *Comput. Chem. Eng.* **2024**, *181*, 108554.
23. Camacho, E.F.; Alamo, T.; de la Peña, D.M. Fault-tolerant model predictive control. In Proceedings of the 2010 IEEE 15th Conference on Emerging Technologies and Factory Automation (ETFA 2010), Bilbao, Spain, 13–16 September 2010; pp. 1–8.
24. Hill, E.; Newton, A.; Gadsden, S.A.; et al. Tube-based robust model predictive control for fault tolerance. *Mechatronics* **2023**, *95*, 103051.
25. Zhang, F.; Wang, L. Disturbance rejection design for Gaussian process-based model predictive control using extended state observer. *Comput. Chem. Eng.* **2024**, *186*, 108708.